Geophys. J. R. astr. Soc. (1977) 49, 225–243

Seismic body waves in anisotropic media: synthetic seismograms

Colum M. Keith* *Department of Geophysics, University of Edinburgh, James Clerk Maxwell Building, Edinburgh EH9 3JZ*

Stuart Crampin *Institute of Geological Sciences, Murchison House, West Mains Road, Edinburgh EH9 3LA*

Received 1976 June 14

Summary. Synthetic seismograms and particle motion diagrams are computed for simple, layered Earth models containing an anisotropic layer. The presence of anisotropy couples the *P*, *SV* and *SH* wave motion so that *P* waves incident on the anisotropic layer from below produce *P*, *SV and* small-amplitude *SH* waves at the surface; both the *P* velocity and the amplitudes of the converted phases vary with azimuth. Significant *SH* amplitudes may be generated even when the wavelength of the *P* wave is much greater than the thickness of the anisotropic layer. Incident *SV* or *SH* waves may each generate large amplitudes of both *SV* and *SH* motion. This strong coupling is largely independent of the degree of velocity anisotropy of the medium. The arrivals from short-period *S* waves exhibit *S*-wave splitting, but arrivals from longer period *S* waves superpose into a modified waveform. This strong coupling does not allow the arrival of separate phases with pure *SV* and *SH* polarization except along directions of symmetry where the motion decouples.

1 Introduction

We investigate theoretically the effects of anisotropy in the mantle by calculating synthetic seismograms and particle motion diagrams for simple plane-layered structures incorporating a single layer of anisotropy beneath the Moho. Keith & Crampin (1977a, b, hereafter Papers I and II) calculated reflection and refraction at a plane interface, and transmission of body waves through an anisotropic layer. In this paper, we investigate how the anisotropic effects demonstrated in Papers I and II manifest themselves in synthetic seismograms for a plane, parallel, multi-layered, lossless, anisotropic Earth model.

Velocity anisotropy in the upper crust has long been recognized by exploration seismologists and usually attributed to fine laminations in isotropic structures (Uhrig & Van Melle 1955; Postma 1955). This type of anisotropy can be modelled by a transversely isotropic medium with the unique axis of symmetry in the vertical direction. Robinson & Costain

* Present address: Department of Energy, Mines and Resources, Ottawa, Ontario, Canada.

(1967) have calculated synthetic seismograms for P pulses incident on plane-layered crustal models exhibiting this type of anisotropy, and concluded that only subtle changes are introduced with no distinctive diagnostic features. Such structures exhibit neither azimuthal variations in P_n velocity, as observed in time-term refraction studies (Raitt *et al.* 1969, 1971; Bamford 1973), nor anomalous surface-wave particle motions, as observed for higher-mode surface-wave trains across Eurasia (Crampin 1967, 1975; Crampin & King 1977). To explain these observations we must place anisotropy in the mantle beneath the Moho, but more importantly we require a more general anisotropy, or, at the least, transverse isotropy with a non-vertical axis of symmetry. This kind of anisotropy is probably due to preferred orientation of olivine grains in the rocks composing the sub-Moho layer (Hess 1964; Francis 1969). Francis suggested that a likely configuration for olivine in the upper mantle would be a transversely isotropic form with the a axis horizontal and perpendicular to the spreading centre and the b and c axes randomly aligned.

The most important consequence of more general anisotropy is that body waves no longer have pure P, pure SV, and pure SH particle motions, but motion in the sagittal plane (P and SV motion) will be coupled to the transverse motion (SH). The *sagittal plane* is the vertical plane containing the propagation vector. Some of the consequences of this have been demonstrated in Papers I and II. This paper is concerned with demonstrating these anisotropic effects in synthetic seismograms and attempting to identify those anomalies most diagnostic of anisotropy in the mantle.

2 Computational procedure

The mathematical formulation of reflection and transmission of plane body waves in layered, anisotropic structures has been presented in Papers I and II. This formulation is easily extended to plane, parallel-layered structures with a free surface (Keith 1975).

In the seismograms presented here, the input pulse is of the form

$$u(t) = A \cdot (t/T)^2 \exp[-(\omega t/k)^2] \sin \omega t,$$

where u is the displacement, ω is the angular frequency, t is time, and the constant k controls the damping. A is an amplitude factor, and T is a time constant (given the value unity). For all input pulses, the damping constant is given the value 3 to produce a pulse which is effectively damped to zero after one cycle with a band-limited spectrum of almost zero dc and small, high-frequency content. If the frequency is, say, 1 Hz, we shall, for brevity, call the pulse a 1-s incident pulse.

The structure (Model 1 of Table 1), the input pulse and the anisotropic medium, (001)-cut orthorhombic olivine, can be thought of as simple, physically plausible idealizations of the physical process of teleseismic body waves incident on the crust–mantle system. There is a high-velocity halfspace beneath the olivine to avoid the complication of a low-velocity zone being present for some orientations of olivine and not for others. The simplicity of this model allows easy interpretation of the resulting surface motion. We also plot actual ground motion, rather than convolving the surface motion with the response of a recording system, in order to preserve the simplicity of the seismogram.

The body-wave velocities along the three crystallographic axes of olivine are shown in Fig. 1(a). In all our computations the (001)-plane is horizontal, and, because of the symmetry of olivine, we need investigate only one quadrant of the horizontal plane between the (100) and (010) axes. The initial orientation of the olivine is with the a and c crystallographic axes in the incident plane (an incident plane of symmetry). The olivine is then rotated about the c axis to bring intermediate orientations into the incident plane, and on

Table 1. Structural models used for the calculations.

Model No.	Layer No.	Thickness (km)	α (km/s)	β (km/s)	ρ (gm/cm^3)
1	1	30	7.25	4.2	2.9
	2	30	(001)-cut olivine (Table 2)		3.324
	3		10.0	5.7	3.6
2	1	6.0	5.64	3.47	2.7
	2	10.5	6.15	3.64	2.8
	3	18.7	6.60	3.85	2.85
	4	30.0	(001)-cut transversely isotropic olivine (Table 2)		3.30
	5		8.30	4.7	3.44

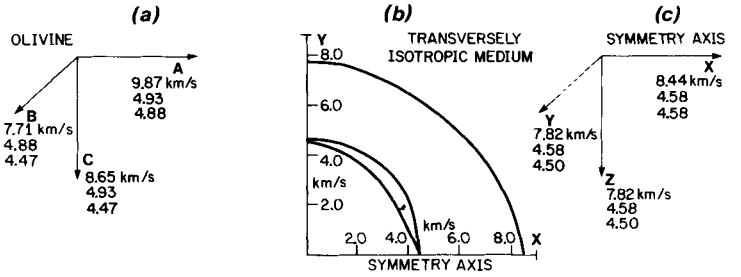

Figure 1. (a) Velocities of the quasi-*P*, and two quasi-shear body waves along the axes of symmetry of olivine. (b) Velocity variation of body waves in the horizontal plane of the transversely isotropic medium. (c) Body-wave velocities along the vertical and horizontal axes of the transversely isotropic medium.

completion of the quadrant the incident plane contains the *b* and *c* crystallographic axes (an incident plane of symmetry).

For comparison with a more realistic model with much less velocity anisotropy, we present some results for Model 2. This model has the crustal parameters of the CANSD model (for the Canadian Shield) of Brune & Dorman (1963) with a modified mantle structure. The anisotropic layer is a more realistic transversely isotropic medium with horizontal axis of symmetry, made up of olivine in a 1 : 2 mix with an isotropic medium (Table 2, Fig. 1). This particular configuration has a compressional wave velocity anisotropy of 7 per cent and a shear wave velocity anisotropy of 4.5 per cent. It should be noted that transversely isotropic olivine, where the *a* axis is the horizontal symmetry axis, has many similarities with (001)-cut olivine, and differences are unlikely to be detected seismically (Crampin 1977). In the calculations presented, using this medium, the symmetry axis is always horizontal. The initial orientation is with the incident plane containing the symmetry axis (an incident plane of symmetry). Again because of symmetry it is necessary to investigate only one quadrant of the horizontal plane.

The procedure for calculating the surface motion has been outlined in Paper II. In order to ensure that the Nyquist frequency, $f_N = 1/2\Delta t$ where Δt is the sampling interval, is large enough to include almost all the frequencies in the input pulse, the sampling rate for all input pulses is made at least eight times the dominant frequency of the input pulse. It is also necessary that the sampling interval in the frequency domain, $\Delta f = 1/T$ where T is the length of the time series, is small enough so that no phase information is lost in a rapidly varying phase spectrum. Physically, this means that the time series must be long enough to include all multiples. For *S* waves incident at near critical angles this has necessitated time series of

at least 1024 s for some examples. At higher angles of incidence and at high frequencies, well known problems of loss of numerical accuracy and overflow are encountered due to the large numbers involved in the layer matrices. These problems are not serious for incident *P* waves because no critical angles are exceeded and the slowness vector remains real valued.

3 Synthetic seismograms for incident *P* pulses

The input pulse for all seismograms has unit magnitude and the seismograms are plotted at the same amplitude scale, which permits a direct comparison of differences in the amplitudes of phases. The incident plane (sagittal plane) for the seismograms is the x–z plane. Different orientations of the anisotropy are examined by rotating the elastic tensor. The seismograms are plotted with radial motion away from the source and vertical motion upwards as positive.

The compressional wave in the anisotropic layer is the quasi-*P* wave (*qP*). The two quasi-shear waves are written *qSV* and *qSH*, depending upon which isotropic shear wave its polarization most nearly resembles. In Papers I and II, it was shown that this nomenclature for transverse waves is not completely satisfactory as for most orientations of the anisotropic medium, the transverse waves have particle motions intermediate between pure *SV* and pure *SH*, and waves can change from *qSV* to *qSH*, and *qSH* to *qSV* as the orientation changes. Nevertheless, the *qSV* and *qSH* notation has certain advantages and will be retained.

A number of examples will be presented for Model 1. The anisotropic medium in this model is olivine (Table 2), with the (001)-cut horizontal. This cut is the plane of symmetry of olivine with most velocity anisotropy (22 per cent for *qP* and 14 per cent for *qSV*) and well illustrates the anisotropic effects.

Table 2. (a) Elastic constants of orthorhombic olivine (Verma 1960). (Density = 3.324 g/cm³.)

$c_{1111} = 324.0$	$c_{2222} = 198.0$	$c_{3333} = 249.0 \times 10^9\,\mathrm{N\,m^{-2}}$
$c_{1122} = 59.0$	$c_{2233} = 78.0$	$c_{3311} = 79.0$
$c_{1212} = 79.3$	$c_{2323} = 66.7$	$c_{1313} = 81.0$

(b) Elastic constants of anisotropic layer in model 2 of Table 1. The material is composed of 1/3 transversely isotropic olivine (*b* and *c* crystallographic axes randomly distributed about the *a* axis) and 2/3 isotropic medium ($\rho = 3.3$, $\alpha = 7.6$, $\beta = 4.4$). (Density = 3.31 g/cm³.)

$c_{1111} = 235.072$	$c_{2222} = 201.572$	$c_{3333} = 201.572 \times 10^9\,\mathrm{N\,m^{-2}}$
$c_{1122} = 64.888$	$c_{2233} = 67.888$	$c_{3311} = 64.888$
$c_{1212} = 69.309$	$c_{2323} = 66.842$	$c_{1313} = 69.309$

Fig. 2(a) shows the surface motion due to a 1-s *P* pulse, incident at 30° with respect to the vertical, arriving at a range of azimuths between two orthogonal symmetry planes. The top and bottom sets of three-component synthetic seismograms are for incident planes of symmetry. Only for such incident planes are the polarizations of the wave in the olivine pure *P*, pure *SV* and pure *SH*, and the incident *P* wave does not generate any *SH* motion. However, the velocity variation, and consequent changes in impedance contrast at the layer boundaries, causes a pronounced variation in the amplitudes of the converted waves. The amplitudes of the second and third arrivals, for example, are smaller and greater, respectively, by more than a factor of three.

Away from incident planes of symmetry, the anisotropy introduces small-amplitude *SH* arrivals on the transverse component seismograms. The first arrival is generated at the upper interface of the olivine layer ($P \rightarrow qP \rightarrow SH$) and the second is the superposition of two

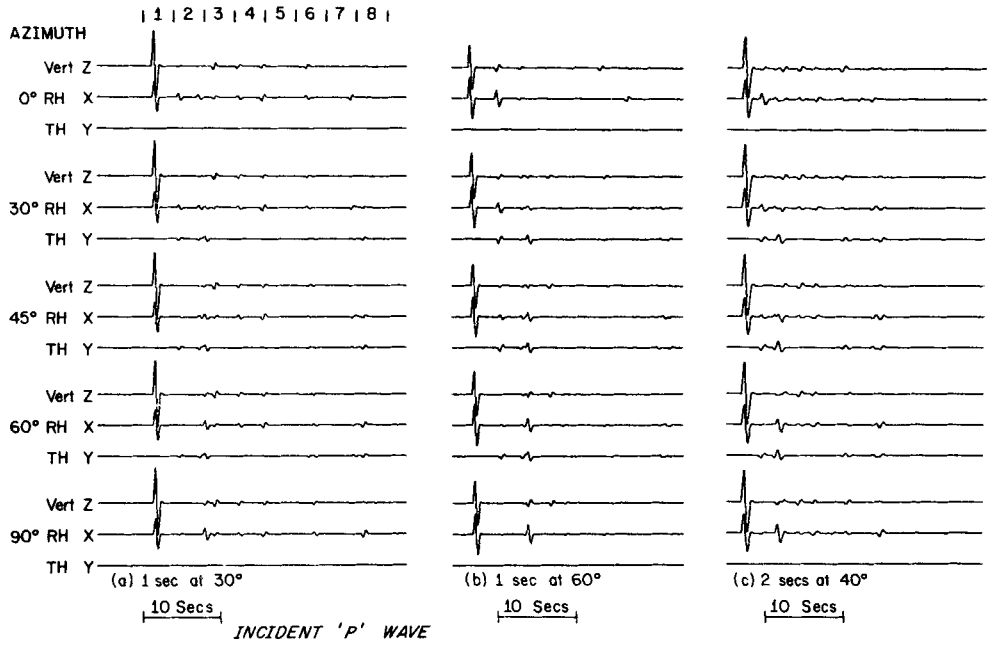

Figure 2. Surface motion produced by a *P* pulse (a) of 1-s period at 30° angle of incidence, (b) of 1-s period at 60° angle of incidence, and (c) 2-s period at 40° angle of incidence on (001)-cut olivine in Model 1 of Table 1. The three components are vertical, radial horizontal (RH), and transverse horizontal (TH). The five three-component sets are at azimuths of 0°, 30°, 45°, 60° and 90° measured from (100) towards (010).

pulses generated at the lower interface, namely ($P \rightarrow qSV \rightarrow SH$, and $P \rightarrow qSH \rightarrow SH$). The difference in velocities of the *qSV* and *qSH* waves in the olivine cause the two pulses to arrive at slightly different times. This phenomenon of double pulse arrivals has been discussed in Paper II. The small amplitude *SH* arrivals occurring later are reverberations within the olivine layer.

Fig. 3 shows five sets of vertical and horizontal particle motion diagrams that correspond to the five sets of three-component seismograms shown in Fig. 2(a). The number in the lower right-hand corner of each plot is the factor by which the particle motions have been amplified to make them clearly visible.

A marked feature of the particle motion diagrams is the cruciform character of many of the plots. The *qP*, *qSV* or *qSH* waves propagating in the olivine layer may each generate all three polarizations *P*, *SV* and *SH* on emerging into an isotropic medium again. These different polarizations are generally separated in time by the different *qSH* and *qSV* delays through the anisotropic layer, and by the different *P* and *S* delays through the crust. This often results in two pulses with different polarizations arriving at the surface with small time separation, and produces the characteristic cruciform appearance of so many of the particle motion diagrams, where two phases with orthogonal polarization arrive in a 4-s window with little overlap in time. It should be noted that the shear waves in the isotropic crust retain the polarizations of the quasi-shear waves from which they were converted, so that the horizontal motion in Fig. 3 reproduces, with little alteration, the polarizations at the upper anisotropic–isotropic interface.

Fig. 3 shows that the motion is confined to the sagittal plane only for incident planes of symmetry. Although the anisotropy bends the *P* ray out of the sagittal plane at the lower

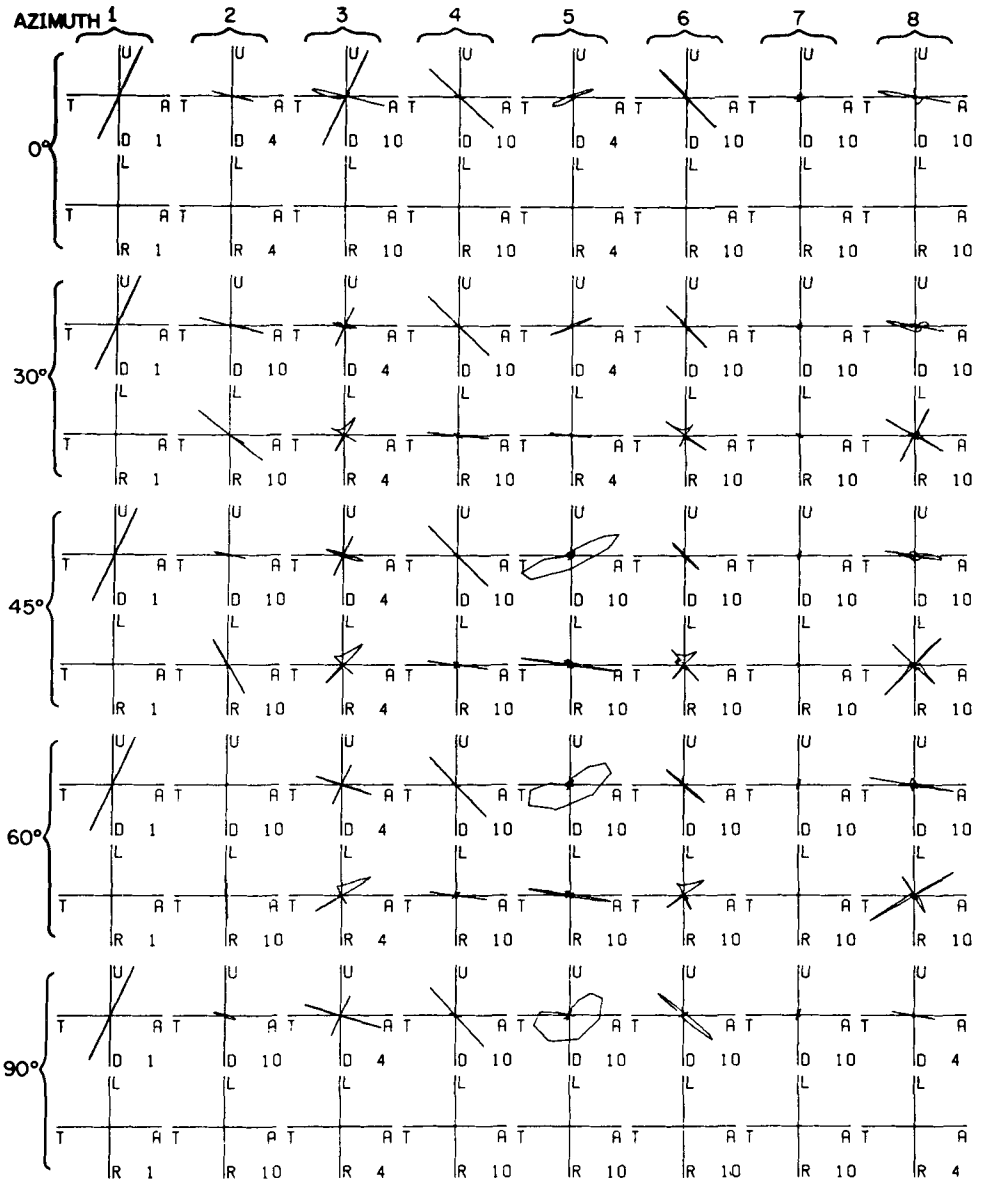

Figure 3. Particle motion diagrams corresponding to the seismograms of Fig. 2(a). There are five sets of vertical and horizontal particle motions corresponding to the five azimuths in Fig. 2(a). For each set of three-component seismograms, 32 s of motion are plotted in consecutive 4-s intervals indicated at the top of Fig. 2(a). The integer in the lower right-hand corner of each plot indicates the scaling factor for each 4-s section. The radial horizontal motion is marked T, A (towards and away from source), the transverse horizontal L, R (left and right and right of propagation director) and the vertical U, D.

olivine interface for all non-symmetry incidence (Paper I), at the upper interface the ray is bent back into this plane, thus the motion of the main *P* arrival (the first column of particle motions in Fig. 3) is always confined to the incident plane. The transverse motion within the anisotropic layer is converted into a shear wave which forms the second arrival. The particle motion of this second arrival is shown in the second column of Fig. 3. For incident planes of

symmetry, this second arrival is an *SV* wave (the polarization is not perpendicular to the previous *P* arrival because the angles of emergence are different). The horizontal particle motion is no longer in the sagittal plane for off symmetry planes of incidence. As the orientation of the olivine changes, the polarization becomes more *SH*-like, with a larger transverse component.

The third column in Fig. 3 has cruciform patterns on the horizontal and vertical sections. These are the result of three arrivals: a *P* wave whose horizontal motion is largely radial and is not visible on the horizontal section, and the double shear arrival discussed above, which is not separated on the sagittal section. Here it is clearly seen that this double-shear arrival is composed of two shear waves with particle motions at right angles to each other having both *SH*-type and *SV*-type motion. Such double-arrival shear waves are also shown in columns 6 and 8, which show the particle motions of the *SV* and *SH* reverberations.

At larger angles of incidence with respect to the vertical, the *SH*-component arrivals have larger amplitudes as shown in Fig. 2(b). In Fig. 2(a), the amplitudes of the first and second *SH* arrivals for the 45° azimuth are 6 and 11 per cent, respectively, of the amplitude of the main *P* phase on the vertical component. In Fig. 2(b), they have increased to 16 per cent and 22 per cent, respectively. This is partly due to the smaller (by 30 per cent) vertical component of the *P* phase at 60° angle of incidence, but also due to more energy going into the *SH* conversions. The first *SH* arrival in Fig. 2(b) is greater than that shown in Fig. 2(a) by 80 per cent, and the second by 40 per cent. More energy goes into the *SH* components because the effective width of the anisotropic layer is greater and because the polarizations of *qSV* and *qSH* are less like pure *SV* and pure *SH* at larger angles of incidence. The azimuthal variation in amplitudes of the second and third arrivals on the vertical and radial components is also more pronounced.

Fig. 2(c) shows the effect of increasing the period of the input pulse. In Fig. 2(c), for a 2-s pulse, arrivals on the horizontal transverse component are of considerable amplitude. For an azimuth of 45°, for example, the second arrival is 25 per cent of the amplitude of the vertical component *P* phase. This is the result of the constructive superposition of the two pulses ($P \rightarrow qSV \rightarrow SH$ and $P \rightarrow qSH \rightarrow SH$) which make up the arrival. In Fig. 2(a), for a 1-s pulse, these two pulses do not overlap (see the particle motion in Fig. 3) and as a consequence no constructive superposition occurs.

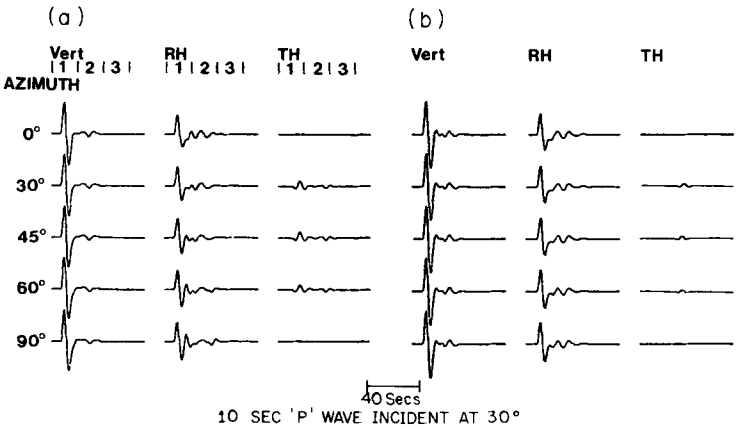

Figure 4. Surface motion produced by a 10-s *P* pulse incident at 30° on (a) Model 1 and (b) Model 2. In (a) the azimuths are as for Fig. 2. In (b) the azimuths are at 0°, 30°, 45°, 60° and 90° measured from the horizontal symmetry axis.

In Fig. 4(a), for a 10-s pulse, the first arrival on the horizontal transverse component is a superposition of three pulses, $P \rightarrow qP \rightarrow SH$, $P \rightarrow qSV \rightarrow SH$, and $P \rightarrow qSH \rightarrow SH$. With increasing period, the amount of generated *SH* energy decreases (Paper II) as the layer thickness becomes a smaller fraction of the wavelength. However, the rate of decrease of the generated *SH* energy, and the constructive superposition of the three pulses is such that, even for long-period *P*, an *SH* arrival of considerable amplitude may be generated. In Fig. 4(a) for the 45° azimuth, the *SH* arrival is 18 per cent that of the vertical component *P* phase.

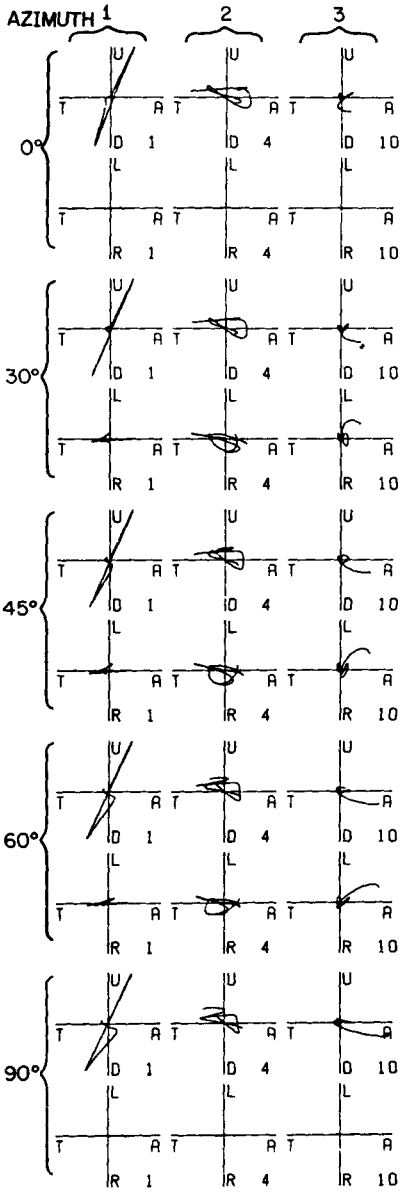

Figure 5. Particle motions corresponding to Fig. 4(a). There are five sets of vertical and horizontal particle motions corresponding to the five azimuths in Fig. 4(a). 60 s of motion are plotted in consecutive 20-s intervals.

The particle motions corresponding to Fig. 4(a) are shown in Fig. 5. Each particle motion plot contains 20 s of motion. For incident planes of symmetry (top and bottom sets of particle motion) no *SH* energy is generated and the motion is confined to the sagittal plane. Off incident symmetry planes, the motion of the *P* phase begins in the sagittal plane, and, as the emergent *SH* phase arrives, rotates out of this plane. The cruciform character of the particle motion plots of the short-period *P* wave in Fig. 3 is not present in this figure, because, with the longer period, the separate pulses overlap.

To study these effects for a more realistic medium with much less velocity anisotropy, we have examined Model 2 of Table 1. For a 1-s input pulse, the maximum amplitude of generated *SH* arrivals is 4 per cent, which on a noiseless synthetic seismogram is barely visible, and we have not presented these figures here. However, for a 10-s input wave, Fig. 4(b), the magnitude of the *SH* arrival is still 8 per cent that of the vertical-component *P* phase, corresponding to the 18 per cent in the purely olivine structure used for Fig. 4(a). Such a transverse component is frequently recorded for 15–20 s period *P* phases at NORSAR, which can only be partially accounted for by scattering processes (Berteussen, private communication). A 15-s *P* wave has a wavelength in the upper mantle of about 120 km. For scattering to have a large effect at such a wavelength, the inhomogeneities would have to be large. The *P–SH* coupling introduced by anisotropy can account for this anomaly with a comparatively thin anisotropic layer.

4 Synthetic seismograms for incident *S* pulses

Fig. 6(a) shows the surface motion for a 1-s *SV* pulse. No anomalous *SH* motion is generated, when the incident plane is a plane of symmetry. Away from such symmetry planes, there is an *SH* arrival on the transverse component with amplitude similar to that of the *SV* arrival.

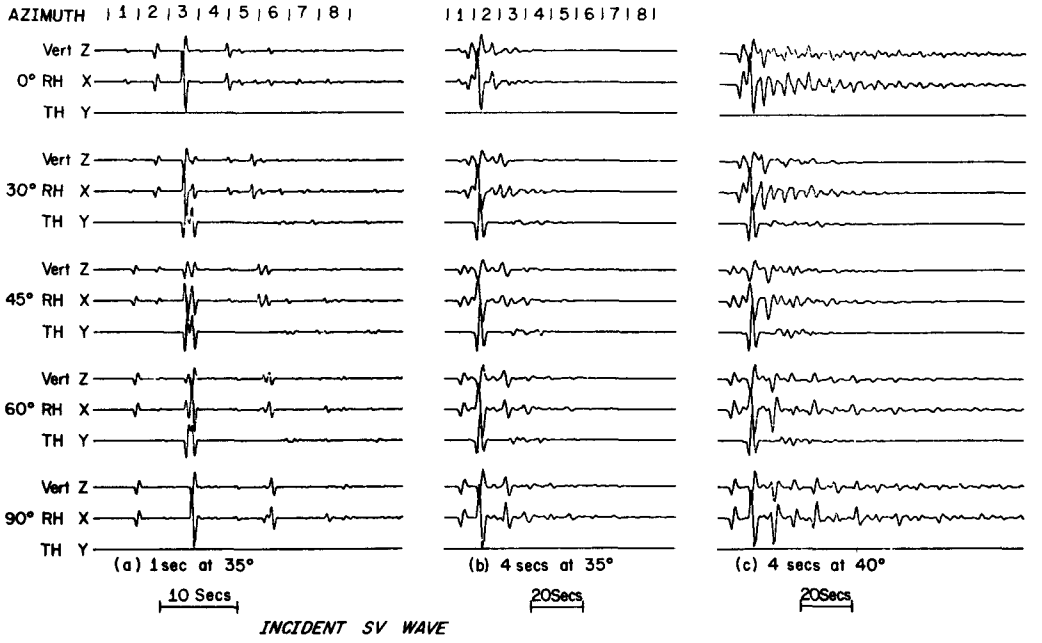

Figure 6. Surface motion produced by an *SV* pulse (a) 1-s period at 35° angle of incidence, (b) of 4-s period at 35° angle of incidence, and (c) 4-s period at 40° angle of incidence in Model 1. The order of seismograms and orientations are as in Fig. 2.

Both of these phases are double pulse arrivals. The *SH* phase, for example, is composed of the pulses $SV \rightarrow qSV \rightarrow SH$ and $SV \rightarrow qSH \rightarrow SH$. The velocity difference between the two quasi-shear waves in the olivine causes these two pulses to arrive at slightly different times and interfere with each other. The resulting waveform (an 'M' shape, for example, for the azimuth of 30°) depends on the time separation of the pulses and also, of course, on the shape of the input waveform. The two precursors to the main arrival are *P* phases generated at the two interfaces ($SV \rightarrow qP \rightarrow P$ and $SV \rightarrow qSV \rightarrow P$). The amplitudes of these two arrivals vary greatly with orientation of the olivine. Other possible precursors have negligible amplitude and are not seen. The most prominent phase following the main *S* arrival is a *P* wave generated at the upper boundary of the olivine (the Moho in this model) by the downgoing *S* wave reflected at the surface. Note how the waveform of this arrival mirrors that of the main *S* arrival. For incident planes of symmetry, this is a single arrival because the *S* phase at the surface is a single arrival. Off incident planes of symmetry, it is a double-arrival *P* wave because the *S* phase at the surface is a double arrival. The arrival time of this phase varies greatly with orientation of the olivine due to the velocity anisotropy of the quasi-shear waves in the olivine. Other much smaller phases on the seismograms are due to further reverberations. To identify these with ray paths requires the calculation of the arrival times of the possible reverberations. For multi-layered media many arrivals are possible. For anisotropic media, the difficulty of this procedure is further compounded because we require the group velocity (the velocity with which energy travels) to determine the speed and direction of the rays in the anisotropic layer. The group velocity is not equal to the phase velocity either in magnitude or direction and is a function of the azimuthal direction.

Fig. 7 shows the particle motions corresponding to the seismograms in Fig. 6(a). The first two columns show the particle motions of the precursor waves. These are clearly *P* waves. However, in column 2 of the 45° and 60° azimuths, the horizontal particle motions indicate a small *SH* component. This motion, barely visible on the seismograms themselves, is due to the phase $SV \rightarrow qP \rightarrow SH$ which has little energy. The third column in Fig. 7 shows the particle motion of the main *S* arrival, which for azimuths of 0° and 90° (incident planes of symmetry), is a pure *SV* wave. Away from incident planes of symmetry, the cruciform character clearly shows a double arrival phase with each arrival having both *SV*-type and *SH*-type motion. The particle motion of the prominent later arrival discussed previously is shown in the fourth and fifth column for the 0° azimuth. The later arrival time shifts the particle motion into the fifth column for the 30° azimuth and the sixth column for the remaining azimuths. The double arrival nature of this phase is most clearly shown for the 45° azimuth.

Fig. 6(b) shows the surface motion for a 4-s *SV* wave. The separate arrivals identifiable in Fig. 6(a) now overlap to produce continuous oscillations both before and after the main *S* arrival. The longer period input pulse ensures that no splitting of arrivals occurs. The waveforms of the *S* wave on the two horizontal components are, however, quite different. Azimuthal variations in the seismograms are marked.

Fig. 8 shows the particle motions corresponding to Fig. 6(b). The particle motion of the main *S* arrival in column 2 of Fig. 8 shows the two pulses, which compose the arrival, combining to produce elliptical motion in the horizontal plane. Motion in the radial vertical plane does, however, remain largely linear. Generally the character of the particle motions is rendered much more perturbed and complicated by the anisotropy.

Fig. 6(c) is again for a 4-s *SV* wave, but at a slightly larger angle of incidence. Reverberations, especially for the incident planes of symmetry, are much more prominent than in Fig. 6(b). The M-shaped main *S* arrival on the radial component is not caused by a double arrival as has been discussed above, since it also occurs for the incident planes of symmetry. This

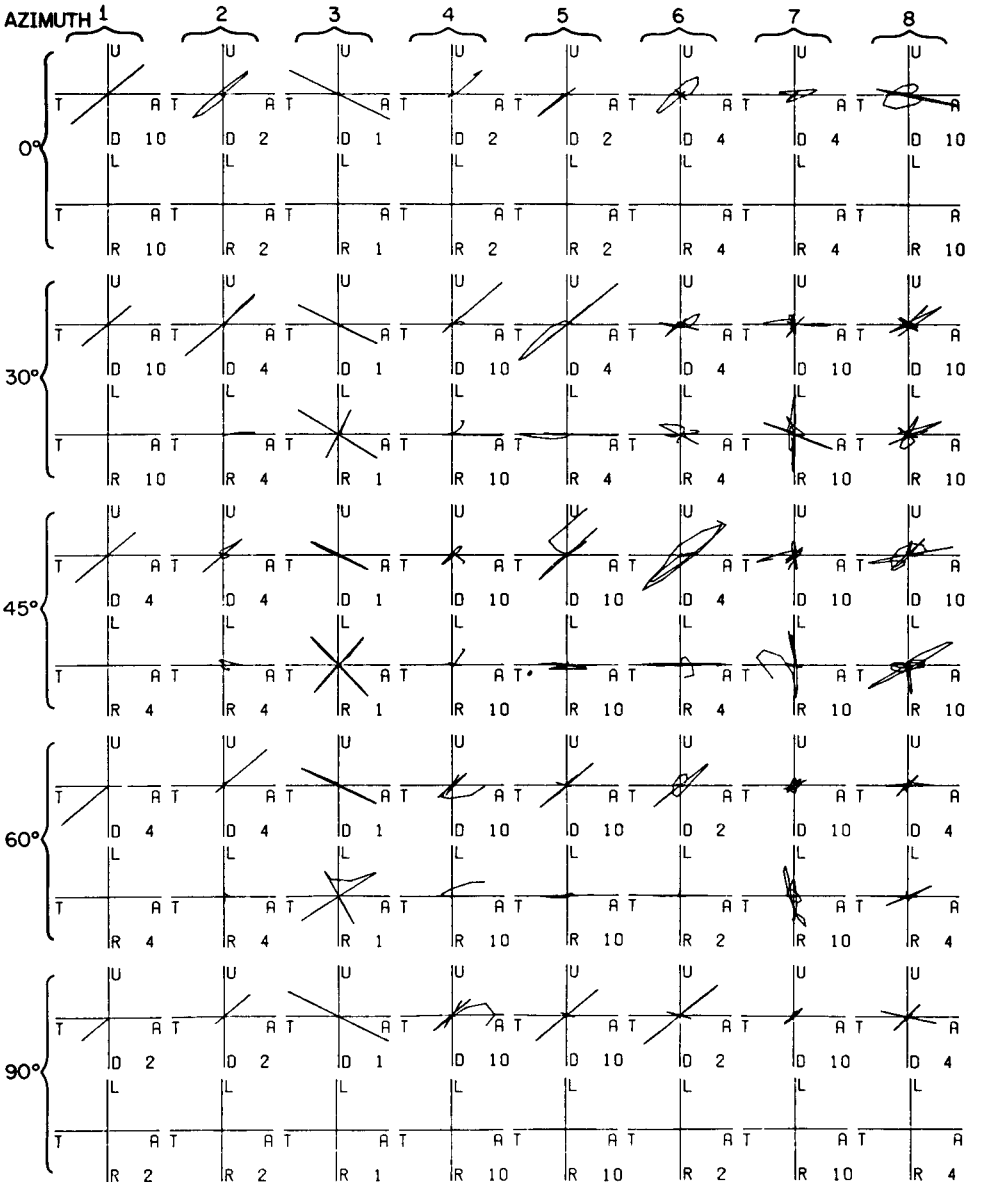

Figure 7. Particle motions corresponding to Fig. 6(a). There are five sets of vertical and horizontal particle motions corresponding to the five azimuths of Fig. 6(a). 32 s of motion are plotted in consecutive 4-s intervals.

M-shaped arrival is composed of the main *S* phase followed closely by the upgoing *P* wave generated at the upper olivine interface by the downgoing *SV* wave reflected at the surface. This serves as a reminder that there are no effects on a single component seismogram uniquely attributable to anisotropy and emphasizes the importance of polarization studies and the consequent necessity of three-component analysis.

The incident *SH* waves in Fig. 9(a) introduce many anomalous phases. For incident symmetry planes, where sagittal and transverse motion is decoupled, the same number of pulses

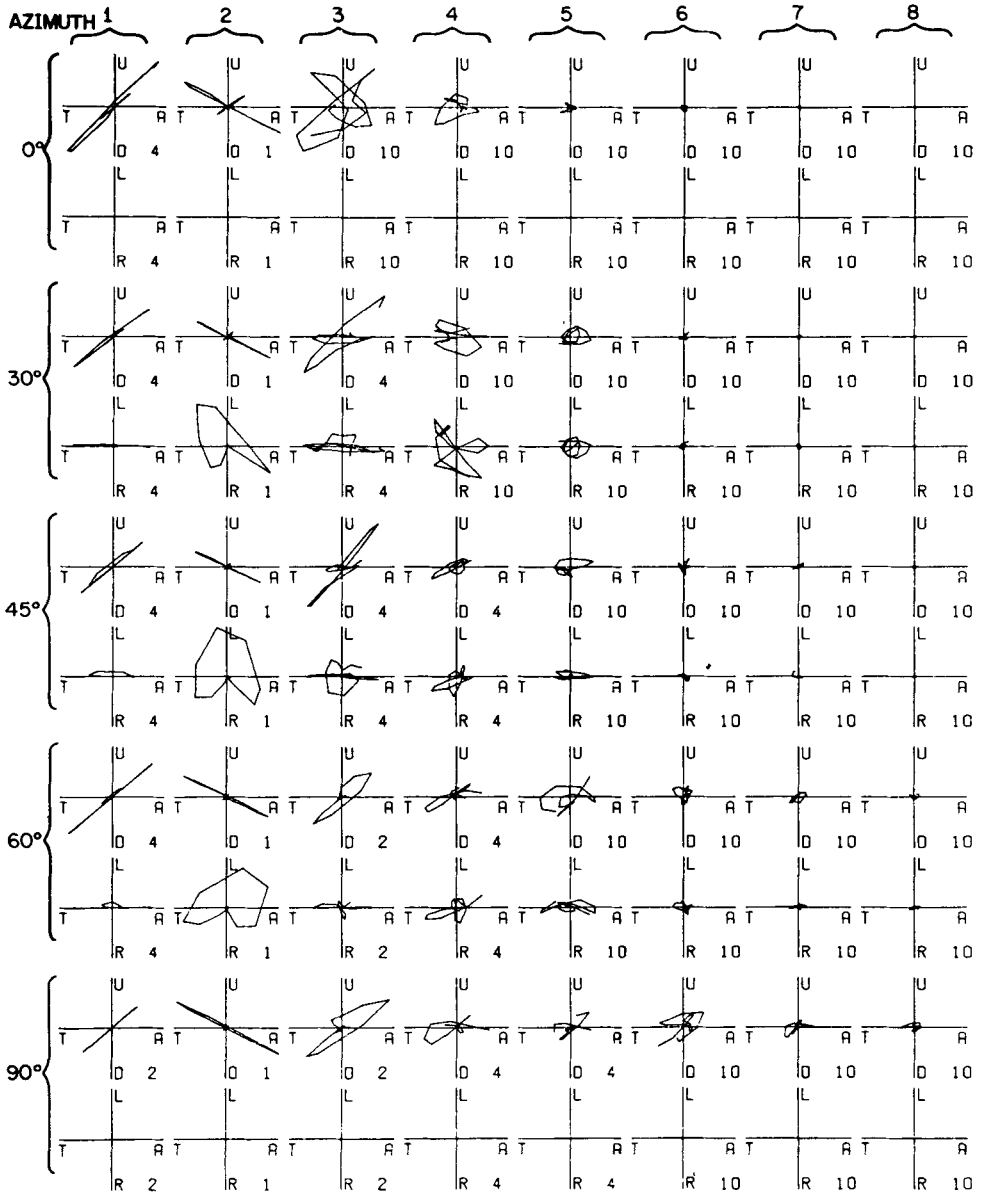

Figure 8. Particle motion plots corresponding to Fig. 6(b). 80 s of motion are plotted in consecutive 10-s intervals.

is generated as for an isotropic structure. Away from such planes, the main arrival is a double-pulse *S* phase with both *SH* and *SV* components. Many of the other arrivals are also composed of double pulses as can be seen from their M-shaped waveforms and the particle motions in Fig. 10. A comparison of Fig. 9(a) with Fig. 6(a) shows that, off incident symmetry planes, the same arrivals are generated for both incident *SV* and *SH* waves, although with different amplitudes and waveforms. The particle motions, in Fig. 10 thus have many characteristics in common with the particle motions for incident *SV* waves, Fig. 7. Away from symmetry planes, the same precursors to the main arrival are seen, the main arrival

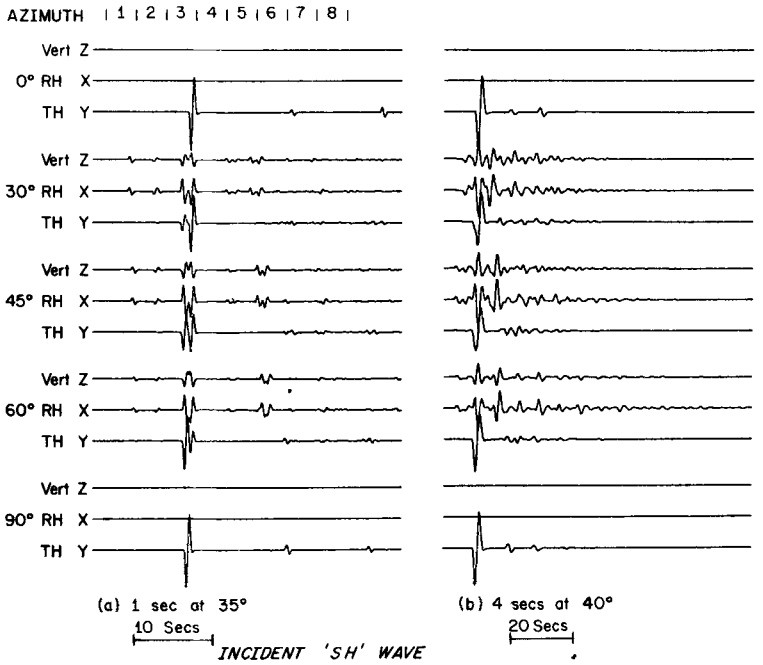

Figure 9. Surface motion produced by an *SH* pulse (a) of 1-s period at 35° angle of incidence and (b) 4-s period of 40° angle of incidence in Model 1. The order of seismograms and orientations as in Fig. 2.

is composed of the two shear waves with polarizations at right angles, and the subsequent arrivals have almost identical polarizations. Fig. 9(b), for a 4-s *SH* wave, emphasizes the high degree of coupling that exists between the sagittal and transverse motion in anisotropic media. For an azimuth of 45°, the amplitude of the *SV* component of the main *S* phase is greater than the *SH* component, and all the reverberations produced by an incident *SV* pulse, Fig. 6(c), are produced again by an incident *SH* pulse.

For incident *P* pulses it has been shown that reducing the level of the velocity anisotropy greatly reduces the amplitudes of the anomalous arrivals. This is not so for incident *S* pulses. Fig. 11(a) and (b) illustrate this by showing the surface motion for incident *SV* and *SH* pulses in Model 2. In Fig. 11(a), a large amplitude *SH* component is generated for an incident *SV* wave, similarly for an incident *SH* wave in Fig. 11(b), large-amplitude *SV* waves are generated for off-symmetry incidence. It appears that reducing the level of velocity anisotropy does little to reduce the coupling between sagittal and transverse motion.

The reason for this observation is instructive. In anisotropic media the polarizations of the *qP* and two quasi-shear waves are mutually orthogonal and fixed with respect to the anisotropic symmetries, no matter how weak the velocity anisotropy (Crampin 1977). Thus the polarization of the quasi-shear waves may be intermediate between *SV* and *SH* (although for convenience we have named them *qSV* and *qSH*). Crampin shows how an incident *SV* or *SH* wave is converted into quasi-shear waves for transmission through an anisotropic solid, but, because of the different *qSV* and *qSH* delays, the original pulse can never quite be reconstructed on entering isotropic media again, and anomalous phases are generated. This type of anomaly exists, however weak the velocity anisotropy, if the anisotropic medium is sufficiently extensive.

The conversion to quasi-shear waves with intermediate polarization also demonstrates why long-period waves are sensitive to comparatively thin anisotropic layers in their path.

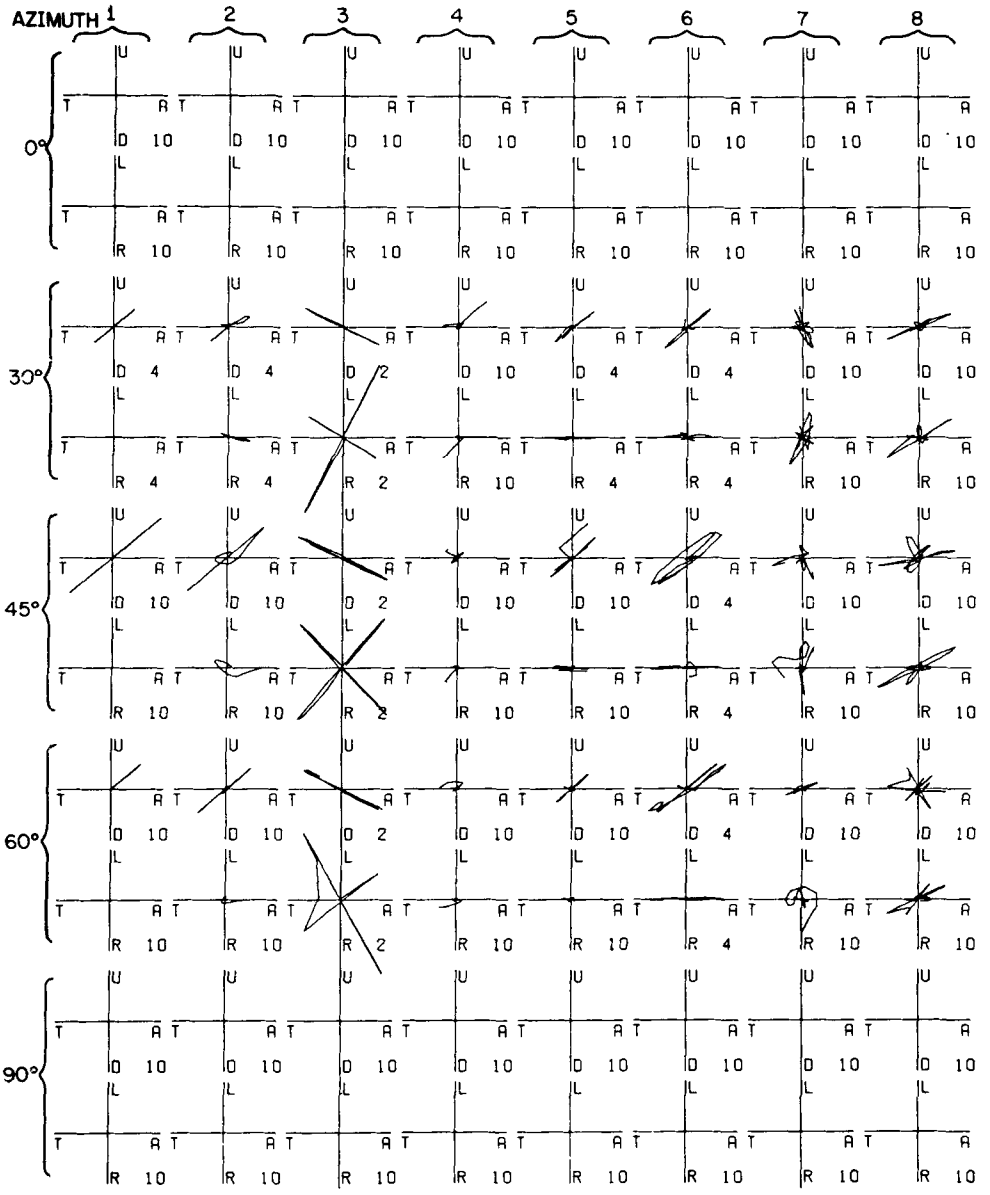

Figure 10. Particle motions corresponding to Fig. 9(a). 32 s of motion are plotted in consecutive 4-s intervals.

Converted to off-axis polarizations on entering the anisotropic layer, the velocity anisotropy ensures that the original pulse can never be completely reconstructed on emergence.

The strong coupling between *SV* and *SH* motion effected by anisotropy means that it is only for incident planes of symmetry, where the sagittal and transverse motions are decoupled, that the *SH* component of the *S* phase can arrive at a different time from the *SV* component. Away from incident planes of symmetry, the shear arrivals contain components of *SV* and *SH* and preserve the polarizations of the quasi-shear from which they were converted. This is clearly illustrated in Fig. 12(a), for an incident *S* pulse with polarization 45° out of the incident plane (that is the input pulse has equal parts of *SV* and *SH* motion). The

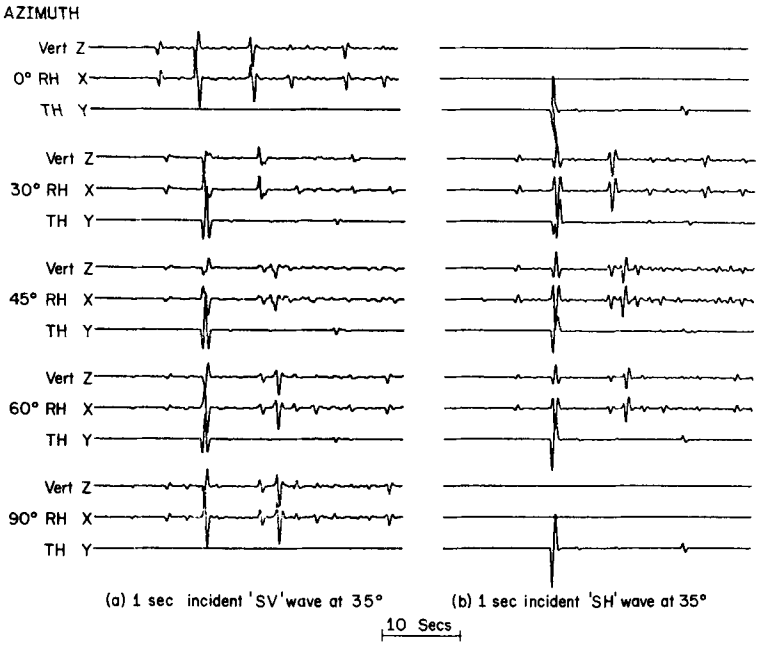

Figure 11. Surface motion produced by (a) 1-s period *SV* pulse at 35° and (b) 1-s period *SH* pulse at 35° angle of incidence in Model 2. The five azimuths are at 0°, 30°, 45°, 60° and 90° measured from the horizontal axis of symmetry.

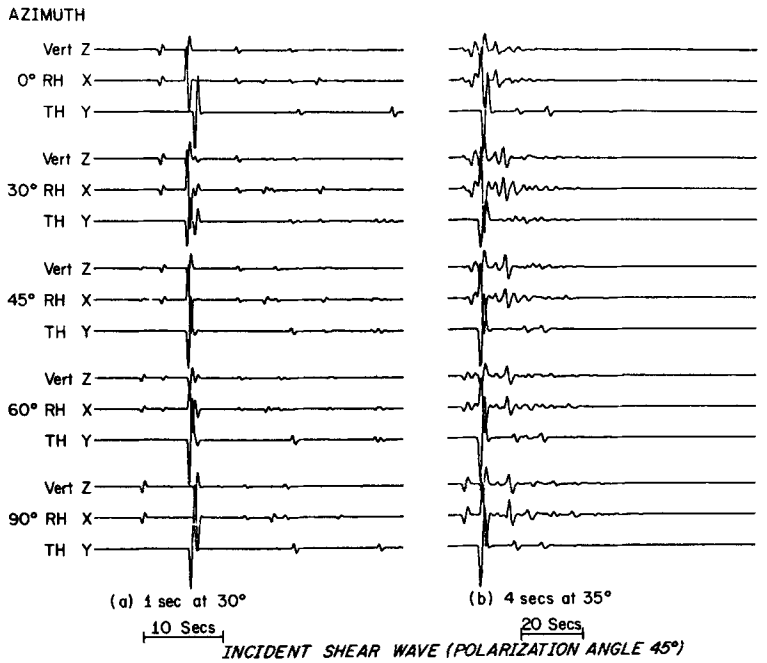

Figure 12. Surface motion produced by an *S* pulse (a) 1-s period at 30° angle of incidence and (b) 4-s period at 35° angle of incidence in Model 1. The input *S* pulse has equal parts *SV* and *SH* motion. The order of seismograms and the orientations are as in Fig. 2.

top set of seismograms clearly shows the *SV* phase arriving before the *SH*. For the other incident plane of symmetry, the *SH* phase precedes the *SV*. For orientations in between, the first swings of the shear arrival are simultaneous on both radial and transverse seismograms. For a longer period input pulse, Fig. 12(b), the peak of the *SH* phase is later than that of the *SV* in the top set of seismograms, and as the orientation changes the *SH* peak gradually overtakes the *SV*. For such longer-period pulses, it is difficult to determine whether the initial swings on the *SV* and *SH* components begin simultaneously, even for incident planes of symmetry, due to the overlapping precursor waves. It is unlikely, therefore, that anisotropy will cause observable *SV* and *SH* phases arriving separately on teleseismic *S* arrivals. For horizontally travelling waves, for example S_n, splitting of the *S* phase into non-simultaneous *SV* and *SH* components has a greater possibility. Such a phenomenon has been discussed by Gupta (1973) and Ryall & Savage (1974) for the S_g phase from anisotropically stressed earthquake regions.

Conclusion

For the numerical models considered, upper mantle anisotropy causes incident *P* waves to generate comparatively small-amplitude *SH* arrivals in the surface motion. A single layer of olivine generates an *SH* pulse at both the upper and lower interfaces, and smaller amplitude reverberations in the layering. The *SH* pulse generated at the lower interface is a double arrival caused by the division of the shear energy between the two quasi-transverse waves in the olivine layer. The amplitudes of the generated *SH* arrivals are strongly dependent on the angle of incidence, generally being greater for greater angles of incidence. All these effects are controlled by the polarization directions of the body waves in the olivine layer, and are of larger magnitude away from incident planes of symmetry. For incident planes of symmetry, the polarizations of the quasi-transverse waves are pure *SV* and pure *SH*, and no anomalous phases are generated. The variation of the particle motion directions with respect to the orientation of the olivine causes variations in the amplitudes of other converted phases.

For long-period *P* waves, the two generated *SH* phases superpose to give a single arrival of significant amplitude. This could be a possible means of identifying anisotropy in the Earth. Scattering of short-period *P* phases by inhomogeneous sub-surface structure would in most cases render the study of transverse motion in the *P* coda of little use for identifying the perturbations resulting from anisotropy. For long-period *P* phases, scattering effects are of smaller magnitude, and *SH* anomalies more diagnostic of anisotropy.

Anisotropy has a pronounced effect on the propagation of *S* waves. The particle motions of the quasi-transverse waves are intermediate between pure-*SV* and pure-*SH* for off-symmetry incident planes. *SV* waves thus generate large-amplitude *SH* arrivals, and vice versa. Both the *SV* and *SH* phases are double arrivals caused by the strong generation of both quasi-shear waves in the olivine layer. If the velocity difference of the quasi-transverse waves is sufficiently large, the phases are split; if it is small, the two pulses superpose and modify the waveform of the arrival. Azimuthal variations in the amplitudes of other converted waves are also produced.

The strong coupling of sagittal and transverse motion in anisotropic media causes the *SH* and *SV* phases at the surface to arrive simultaneously, unless the incident plane is a plane of symmetry. A difference in the arrival times of the *SV* and *SH* components of the *S* phase is more likely for such horizontally propagating *S* waves as S_n (provided the horizontal plane is a plane of symmetry when there is no coupling of *SV* and *SH* motion for propagation parallel to the surface).

The strong coupling of *SV* to *SH*, and the velocity difference between the two quasi-shear waves in the olivine cause complications in the polarization of *S* phases. Focal mechanism solutions using *S*-wave polarizations, for example, will be rendered more difficult. Studies of the polarization of teleseismic *S* phases are potentially of great use in identifying anisotropy in the Earth.

No measurements have been made for models with transition zones rather than discontinuous interfaces. The effects on the direct and converted arrivals would no doubt be slightly modified by the transition zone, but would not be substantially altered as the anomalies are caused by the intrinsic properties of the anisotropic media rather than the interfaces. However, the reverberations, which are a prominent feature of many of the seismograms presented here, are likely to be strongly modified by transition zone interfaces.

It is interesting to compare the kinds of effects produced by anisotropy and by dipping layers. In the latter case, *P* and *SV* waves incident in the up and down-dip directions produce no motion out of the incident plane, and *SH* waves are transmitted as *SH* waves. For waves incident between these two directions, anomalous particle motion is produced because the waves are refracted out of the incident plane with the maximum effect being for incident directions normal to the dip direction. The azimuthal variation thus differs from that due to anisotropy. For an incident *P* wave, the particle motion of the *P* arrival will be off azimuth due to the refraction. We have shown that anisotropy does not produce this effect (unless the recording station is immediately on top of the anisotropy). The shear wave generated at the dipping boundary by an incident *P* wave will have an *SH*-type component due to the refraction. For the delay between the main *P* arrival and this shear wave to be the same as that due to an anisotropic layer in the mantle. the dipping layer must be placed in the mantle. In addition, for incident *SV* (and *SH*) waves to produce shear wave arrivals with large *SH* (and *SV*) components, the angle of dip must be comparatively large. In most areas of the world, the Moho is found to be horizontal or has a small dip angle. Finally, and perhaps most importantly, simple dipping layers cannot produce double-arrival shear waves as exhibited here for anisotropic layers. Polarization studies will clearly separate the effects of anisotropy from those due to dipping layers.

The effects of anisotropy on incident *P* waves are small, while the effects on incident *S* waves are comparatively large. *P* waves are, however, easier to study because *S* waves occur in a comparatively noisy section of the seismogram, contaminated by the *P* coda and signal generated noise. It is thus difficult to predict whether studies of *P* waves or *S* waves are best suited for the identification of anisotropy in the Earth. We have demonstrated, however, that in both cases polarization studies using three-component records will show diagnostic anomalies in the presence of anisotropy.

We have used olivine as the anisotropic medium in this study because it has a large velocity anisotropy and clearly demonstrates the anisotropic effects. We have simulated a weaker velocity anisotropy by using a material composed of one-third transversely isotropic olivine (with horizontal axis) and two-thirds of an isotropic medium. This gives a *P*-velocity anisotropy of 7 per cent, similar to that observed in some oceanic time-term refraction work. The anomalies for incident *P* waves are considerably smaller for this medium, although for long-period *P* they are still significant. There is little diminution in the anomalous behaviour for incident *SV* and *SH* waves. The anomalies demonstrated in this paper are dependent on the polarizations of the shear waves. These anomalies will require rotated, calibrated, and digitized (preferably digitally recorded) three-component records for their recognition. Most seismological results are based solely on the analysis of *P* phases of vertical component records, and it is not surprising that such anomalies have not been recognized before. Even for very weakly anisotropic media, it has been shown (Crampin 1977 and Paper II), that the

magnitudes of the anisotropic effects can be maintained, provided the thickness of the anisotropic layer is sufficient. This is because even a small amount of anisotropy removes the degeneracy that shear waves exhibit in isotropic media, and fixes the polarizations of the quasi-shear waves with respect to the symmetries of the medium.

Acknowledgments

This work was begun while CMK was at the Department of Geophysics, Edinburgh University, and completed whilst he was a Post-doctoral Fellow of the National Research Council of Canada in the Division of Seismology and Geothermal Studies of the Earth Physics Branch, the Department of Energy, Mines and Resources. The work undertaken by SC was part of the research programme of the Institute of Geological Sciences and is published with approval of the Director, IGS.

References

Bamford, S. A. D., 1973. Refraction data in Western Germany – A time-term interpretation, *Z. Geophys.*, **39**, 907–927.

Brune, J. N. & Dorman, J., 1963. Seismic waves and Earth structure in the Canadian Shield, *Bull. seism. Soc. Am.*, **53**, 167–210.

Crampin, S., 1967. Coupled Rayleigh–Love second modes, *Geophys. J. R. astr. Soc.*, **12**, 229–235.

Crampin, S., 1975. Distinctive particle motion of surface waves as a diagnostic of anisotropic layering, *Geophys. J. R. astr. Soc.*, **40**, 177–186.

Crampin, S., 1977. A review of the effects of anisotropic layering on the propagation of seismic waves, *Geophys. J. R. astr. Soc.*, **49**, 9–27.

Crampin, S. & King, D. W., 1977. Evidence for anisotropy in the upper mantle beneath Eurasia from the polarization of higher mode seismic surface waves, *Geophys. J. R. astr. Soc.*, **49**, 59–85.

Francis, T. J. G., 1969. Generation of seismic anisotropy in the Upper Mantle along the mid-oceanic ridges, *Nature*, **221**, 162–165.

Gupta, I. N., 1973. Premonitory variations in *S*-wave velocity anisotropy before earthquakes in Nevada, *Science*, **182**, 1129–1132.

Hess, H., 1964. Seismic anisotropy of the uppermost Mantle under ocean, *Nature*, **2**, 629–631.

Keith, C. M., 1975. Propagation of seismic body waves in layered anisotropic structures, *PhD dissertation*, Edinburgh University.

Keith, C. M. & Crampin, S., 1977a. Seismic body waves in anisotropic media: reflection and refraction at a plane interface, *Geophys. J. R. astr. Soc.*, **49**, 181–208.

Keith, C. M. & Crampin, S., 1977b. Seismic body waves in anisotropic media: propagation through a layer, *Geophys. J. R. astr. Soc.*, **49**, 209–223.

Postma, G. W., 1955. Wave propagation in a stratified medium, *Geophys.*, **20**, 780–806.

Raitt, R. W., Shor, G. G., Francis, T. J. G. & Morris, G. B., 1969. Anisotropy of the Pacific Upper Mantle, *J. geophys. Res.*, **74**, 3095–3109.

Raitt, R. W., Shor, G. G., Morris, G. B. & Kirk, H. K., 1971. Mantle anisotropy in the Pacific Ocean, *Tectonophys.*, **12**, 173–186.

Robinson, E. S. & Costain, J. K., 1967. Surface motion from pulse transmission through anisotropic layered structures, *Bull. seism. Soc. Am.*, **57**, 983–990.

Ryall, A. & Savage, W. U., 1974. *S* wave splitting: Key to earthquake prediction? *Bull. seism. Soc. Am.*, **64**, 1943–1951.

Uhrig, L. F. & Van Melle, F. A., 1955. Velocity anisotropy in stratified media, *Geophys.*, **20**, 774–779.

Verma, R. K., 1960. Elasticity of some high density crystals, *J. geophys. Res.*, **65**, 757–766.

Note added in proof

The reverberations (and non-linear particle motion) of the seismograms in Fig. 6(c) are caused by the angle of incidence of the long-period SV wave exceeding the critical angle at the base of the anisotropic layer. Nuttli (1961) and Nuttle & Whitmore (1962) discuss non-linear S motion for isotropic surface structures. When the critical angle is exceeded the excitation factors of the derived waves are complex and translate directly to differences in phase between the three components of displacement and non-linear particle motion. The vertical components of the slowness vectors of the derived compressional waves are complex and surface waves will be generated. If these slowness vectors are imaginary the motion is tied to the interface and decreases exponentially with depth. However, chance solution of the normal mode boundary conditions will be rare, and the slowness vectors are usually complex and energy will leak into the halfspace. In both cases energy is trapped in the layering leading to reverberations. Isotropic SH waves cannot reverberate in this way, but the $SH \rightarrow qSV$ conversions at isotropic/anisotropic interfaces (where there is no saggittal symmetry) produces SV motion which reverberates under the same conditions (compare Figs 6(c) and 9(b)).

Nuttli, O. W., 1961. The effect of the Earth's surface on the S wave particle motion, *Bull. seism. Soc. Am.*, **51**, 237–246.

Nuttli, O. W. & Whitmore, J. D., 1962. On the determination of the polarization angle of the S wave, *Bull. seism. Soc. Am.*, **52**, 95–107.